\$ SUPER

Contents lists available at ScienceDirect

# **Atmospheric Environment**

journal homepage: www.elsevier.com/locate/atmosenv



# Investigation of coastal ammonium aerosol sources in the Northwest Pacific Ocean

Alexandra B. MacFarland <sup>a,\*</sup>, Emily E. Joyce <sup>a</sup>, Xuchen Wang <sup>b</sup>, Wendell W. Walters <sup>a</sup>, Katye E. Altieri <sup>c</sup>, Hayley N. Schiebel <sup>d</sup>, Meredith G. Hastings <sup>a</sup>

- <sup>a</sup> Institute at Brown for Environment and Society and Department of Earth, Environmental, and Planetary Sciences, Brown University, 324 Brook Street, Box 1846, Providence, RL 02912, USA
- <sup>b</sup> Marine Organic Geochemistry, Ocean University of China, 238 Songling Road, Qingdao, China
- <sup>c</sup> Department of Oceanography, University of Cape Town, Rondebosch, Cape Town, 7700, South Africa
- d Center for Urban Ecology and Sustainability, Suffolk University, 8 Ashburton Place, Boston, MA, 02108, USA

#### HIGHLIGHTS

- Nitrogen deposition to the Pacific Ocean is linked to biogeochemical changes.
- Observations include year-round ammonium concentration and isotopes, transport analysis, and aerosol composition.
- Together with an isotope mixing model results suggest ammonium is mainly from agriculture/animal husbandry.
- Seasonally the highest ammonium concentration and aerosol loading occurs in winter.
- Source contributions are critical to determine if external N is shifting ocean biogeochemistry.

#### ARTICLE INFO

Keywords: Ammonium Isotopes Deposition Ocean Anthropogenic

#### ABSTRACT

Determining the magnitude and origins of nitrogen (N) deposition in the open ocean is vital for understanding how anthropogenic activities influence oceanic biogeochemical cycles. Excess N in the North Pacific Ocean (NPO) is suggested to reflect recent anthropogenic atmospheric deposition from the Asian continent, changes in nutrient dynamics due to marine N-fixation, and/or lateral transport of nutrients. We investigate the impact of anthropogenic and marine sources on reactive N deposition in the NPO, with a focus on ammonium (NH<sub>4</sub><sup>+</sup>), an important bioavailable nutrient, using aerosol samples (n = 108) collected off the coast of China (Changdao Island). This study site is used as a proxy for continental emissions that can be exported and subsequently deposited to the ocean. The NH $_{+}^{+}$  concentration of aerosol samples varied seasonally (p < 0.05), with a higher average value in winter  $(2.8 \pm 1.1 \, \mu \text{g/m}^3)$  and spring  $(1.9 \pm 0.8 \, \mu \text{g/m}^3)$  compared to autumn  $(0.7 \pm 0.6 \, \mu \text{g/m}^3)$ and summer  $(1.4 \pm 0.4 \,\mu\text{g/m}^3)$ . The isotopic composition of aerosol NH<sub>4</sub> varied seasonally, with higher averages in spring (13.3  $\pm$  7.9%) and summer (15.6  $\pm$  6.2%) compared to autumn (3.2  $\pm$  2.5%) and winter (3.8  $\pm$  11.4 ‰). These seasonal patterns in the isotopic composition of NH<sup>+</sup><sub>4</sub> are investigated based on correlations of aerosol chemical species, seasonal shifts in transport patterns, partitioning of ammonia/ammonium between the gas and particle phase, and continental versus marine sources of ammonia. We find that anthropogenic activities, mainly agricultural practices (e.g., volatilization, fertilizer, animal husbandry), are the primary sources of NH<sup>+</sup><sub>4</sub> deposited to the NPO.

#### 1. Introduction

Nitrogen (N) deposition in the ocean has been increasing since preindustrial times (Galloway et al., 2004). As a result, coastal studies have observed eutrophication (rapid growth and decay), algal blooms, and oxygen minimum zones. However, the consequences to the open ocean (characterized here as particulate matter that can be exported and deposited into the ocean) are less well-known. Global modeling suggests

<sup>\*</sup> Corresponding author. 324 Brook Street, Box 1846, Providence, RI, 02912, USA. *E-mail address:* alexandra macfarland@brown.edu (A.B. MacFarland).

anthropogenic inputs have recently led to an overall increase in ocean carbon sequestration of  $\sim\!0.4\%$ , which is equivalent to an uptake of about 0.15 Pg C yr $^{-1}$  (Jickells et al., 2017). Another study suggests that excess N could shift nutrient limitations from N to phosphorus, which could change the composition of phytoplankton species as well as the structure of ecosystems in the ocean (Elser et al., 2009). Additionally, an increase in primary productivity from excess N could expand low oxygen zones (Jickells et al., 2017). The continued addition of N from anthropogenic activities, mostly land-based activities, has the potential to alter oceanic, and even global, biogeochemical systems (Jickells et al., 2017), such that identifying potential N trends and source contributions over time could help influence emissions reduction policies and/or mitigation strategies.

Inorganic N (nitrate (NO $_3$ ), nitrite (NO $_2$ ), and ammonium (NH $_4$ )) is the main form of N deposition in polluted (Cornell et al., 2003; Russell et al., 1998) as well as remote locations (Duce et al., 2008; Galloway et al., 1982, 1989, 1996). Distinguishing amongst the sources of N deposition to the open ocean is vital for discerning the effects of human activities on biogeochemical cycles (Altieri et al., 2021). If the deposition is a consequence of terrestrial/continental emissions, it signifies an outside input to the open ocean, and if that input is influenced largely by anthropogenic activities, it may continue to rise over time (Duce et al., 2008; Seinfeld and Pandis, 2012; Jickells et al., 2017). On the other hand, if the N is coming from the ocean itself and cycling through the atmosphere prior to (re)deposition, it would not be considered a net input of N to the ocean.

Excess N has been observed in the Northwest Pacific Ocean (Kim et al., 2011), but there are conflicts as to origin of this excess. Excess N is quantified as relative to the expected ratio of nitrogen to phosphorus in the open ocean (i.e.,  $N^* = N - (R_{N:P}) \times P$ ; where  $R_{N:P}$  is the ratio of nitrogen to phosphorus; Gruber and Sarmiento, 1997). In the Northwest Pacific, excess N (i.e., +N\*) has been reported and based on the geographical patterns, rates of change in N\*, and the time frame of increases in oceanic N, it was concluded that the excess N was due to deposition of anthropogenic reactive N emissions from the Asian continent (Kim et al., 2011, 2014). However, this finding requires that all N deposition is considered external to the ocean's N budget and requires limited change in N-fixation over the same time period. At Station ALOHA in the North Pacific Ocean (NPO; 22.75°N, 158.00°W; Quay et al., 2010) only about 75% of the N measured could be accounted for via N-fixation (Karl et al., 2012) and mesoscale mixing (Johnson et al., 2010), and it is possible that atmospheric deposition may explain the remaining 25%. Additionally, a modeling study of gyres in the subtropics explains nutrient dynamics due to changes in marine N-fixation or lateral transport of nutrients (Letscher et al., 2016).

Stable isotopic composition of N holds promise as a valuable tool for identifying and detailing the sources and chemistry of reactive N. Different sources of NH<sub>x</sub> (NH<sub>4</sub> and ammonia (NH<sub>3</sub>)) exhibit unique isotopic signatures (Altieri et al., 2014, 2021). For example, continental and marine aerosol NH<sub>4</sub><sup>+</sup> have different observed compositions of  $\delta^{15}$ N (Jickells et al., 2003). (The nitrogen stable isotopic composition is determined as follows:  $\delta^{15}N$  (%) =  $[(^{15}N/^{14}N)_{sample}/(^{15}N/^{14}N)_{standard}$  -1]  $\times$  1000, where the N isotopic reference is air-N<sub>2</sub>). Physical, chemical, and biological processes differentiate between the two isotopes (15N and  $^{14}$ N) which lead to small but measurable differences in the ratio of  $^{15}$ N to <sup>14</sup>N among the forms of N found in the environment via various sources (Sigman and Fripiat, 2019). Many studies have focused on the deposition flux of  $NO_3^-$  and  $\delta^{15}N-NO_3$ , we seek to add to our understanding of NHx since NHx is readily bioavailable and its overall loading in the atmosphere has increased over time (Altieri et al., 2021). NH<sub>4</sub><sup>+</sup> is a bi-product of NH<sub>3</sub> emissions; natural sources of NH<sub>3</sub> to the atmosphere include N-fixation, organism waste, and decomposition, while anthropogenic sources include fertilizer, livestock, and industrial processes (Zhao et al., 2015).

Using stable isotopes, transport patterns, and the composition of wet deposition (rainwater) observations from Bermuda, Altieri et al. (2013,

2014) were able to distinguish sources of  $NH_4^+$  and  $NO_3^-$  in the western North Atlantic Ocean. The island of Bermuda encounters continental as well as oceanic-influenced air masses. For  $NO_3^-$ , an anthropogenic imprint was determined via lower  $\delta^{15}N$  values and higher concentrations in continental air masses. For  $NH_4^+$ , there was no correlation between  $\delta^{15}N-NH_4^+$  and air mass history, and simple modeling was able to account for both the concentration and isotopic composition of  $NH_4^+$  in precipitation with marine emissions as a primary source (Altieri et al., 2014). Overall, the Bermuda work determined that 27% of total N wet deposition (inorganic + organic; Altieri et al., 2016) was anthropogenic in origin, which contrasts with global models (Jickells et al., 2017) that suggest as much as 75% of N deposition to the oceans represents an external (anthropogenic) source of oceanic N.

This current study has two main objectives, (1) to understand and quantify the influence of anthropogenic emissions of reactive N on atmospheric NH $_4^+$  and (2) to determine the atmospheric composition and sources of NH $_4^+$  to the NPO with a focus on seasonal trends. Aerosol samples were collected on Changdao Island, China for the duration of one year from 2020 to 2021. This study site is used as a proxy for continental emissions that can be exported and subsequently deposited to the ocean. We test the hypothesis that N deposition to the NPO is primarily anthropogenic based on continental versus marine sources of NH $_3$ , the isotopic composition of NH $_4^+$ , aerosol chemical composition, seasonal shifts in transport patterns, and partitioning of NH $_3$ /NH $_4^+$  between the gas and particle phases.

#### 2. Methods

#### 2.1. Study site

The sampling site was located on the eastern windward side of Changdao Island (37.92°N, 120.73°E), positioned in the Yellow Sea roughly 64 km from the mainland of China (Fig. 1). The Yellow Sea is bordered by the three peninsulas (Liaodong, Shandong, and Korea), all well populated and industrialized, making the Northern Yellow Sea vulnerable to anthropogenic input (Kurokawa et al., 2013; Luo et al., 2014). Aerosol samples (n = 108; bulk total suspended particles (TSP)) were collected on pre-cleaned TE-G653 Glass Fiber Filters (in compliance with the method of US EPA FRM 40 CFR Part 50 Appendix B) using a high-volume aerosol sampler operating at 1.0 m<sup>3</sup> min<sup>-1</sup> (see further details in Ren et al. (2022)). The samples were collected for either 24, 48, or 72 h. Lab blanks and field blanks were taken, the latter represented a filter placed in the sampler, then removed and processed as a sample. The  $\sim$ 1 m tall tower was placed on a flat cement floor atop a hill with no nearby obstructions (e.g., trees, buildings) and is solely used as an air monitoring station. All filter samples were frozen at  $-20~^{\circ}\text{C}$  after collection and between all analyses. This has been demonstrated to be sufficient for upholding the original chemical composition of aerosol and rainwater samples in previous studies (Seitzinger et al., 2005; Knapp et al., 2010; Altieri et al., 2013, 2014; Gobel et al., 2013).

After the frozen samples were received at Brown University, a 5  $\times$  5 cm square was cut from the center of the filter at room temperature and extracted in a pre-cleaned bottle with  $\sim\!100$  mL of MQ water (exact amounts were recorded via weight) and then sonicated for 1 h. After sonication, the filters were removed, and the samples were frozen at  $-20~^{\circ}\text{C}$  until further analyses.

#### 2.2. Nitrogen concentration analysis

The concentration of ammonium ([NH $_4^+$ ]), nitrate ([NO $_3^-$ ]), and nitrite [NO $_2^-$ ]) were determined colorimetrically (indophenol blue) using a discrete UV–Vis analyzer (Westco Smartchem 200). U.S. EPA Compliant Methods 350.1 (O'Dell, 1993), 353.2 (Revision 2.0), and 354.1 were followed for NH $_4^+$ , NO $_3^-$ , and NO $_2^-$ , respectively. Standard lab protocols were followed, including calibration to standards as well as blanks and in-house quality control measurements. The pooled standard deviation

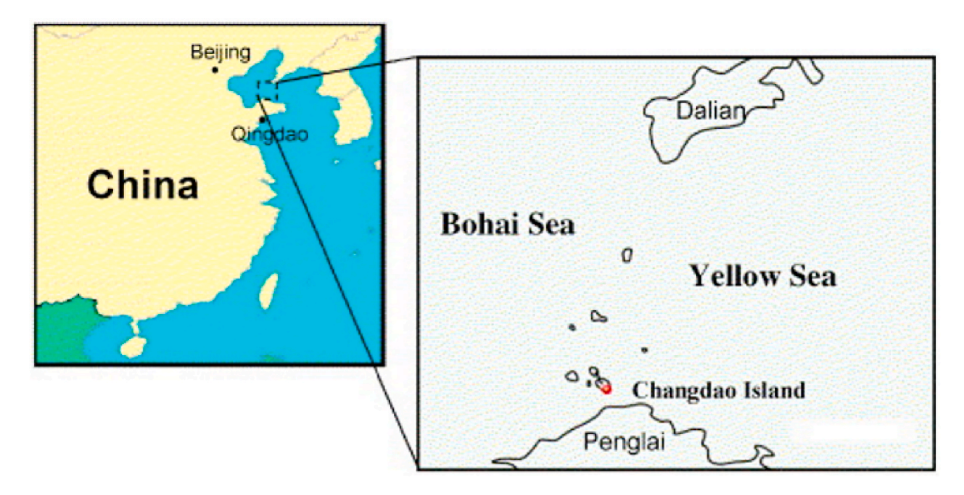


Fig. 1. Map of eastern China and location of sampling on Changdao Island (37.92°N, 120.73°E, red dot).

 $(1\sigma)$  for  $[NH_4^+]$  was 0.6  $\mu$ mol  $L^{-1}$ , and 0.3  $\mu$ mol  $L^{-1}$  for  $[NO_3^-]$  and  $[NO_2^-]$ . Liquid concentrations ( $\mu$ mol  $L^{-1}$ ) were converted to air concentrations ( $\mu$ g m $^{-3}$ ) based on extraction volume (L) and average volume of air sampled through the filter ( $m^3$ ).

# 2.3. Elemental analyses

Concentrations of calcium ( $Ca^{2+}$ ), magnesium ( $Mg^{2+}$ ), sodium ( $Na^+$ ), and potassium ( $K^+$ ) were measured on an Inductively Coupled Plasma (ICP) atomic emission spectrometer. Samples (n=103) were filtered with 0.45- $\mu$ m filters and an aliquot of each sample solution was made 2% acidic with nitric acid. A commercial standard (IV-4) for each specific element was run roughly every 10 samples. The relative standard deviation for the standards was  $\leq 3.3\%$  for all four elements. All samples analyzed were corrected for drift, acidification, and blanks.

## 2.4. Ion analyses

Chloride (Cl<sup>-</sup>) and sulfate (SO<sub>4</sub><sup>2</sup>-) concentrations were measured on an Ion Chromatography (IC) instrument (Dionex Integrion HPIC) using suppressed conductivity detection. (We note here that the aerosol samples were significantly influenced by sea salt and had very high chloride and sulfate content. Those concentrations were significantly higher than nitrate concentrations, making it difficult to accurately detect nitrate peaks on the IC, and we therefore report the UV-Vis analyzer results for nitrate concentrations). Anions were determined using a Dionex AS19-4  $\mu m$  guard (4  $\times$  50 mm) and analytical column (4  $\times$  250 mm) with 20 mM KOH as eluent with a flow rate of 1 mL min<sup>-1</sup>. All samples (n = 100) were filtered with 0.45- $\mu m$  filters before being analyzed. In-house quality control standards (QCs) were run approximately every six samples. The pooled standard deviation for duplicates was 2.0  $\mu$ mol for both Cl<sup>-</sup> and SO<sub>4</sub><sup>2-</sup> (n = 13 pairs and 12 pairs, respectively). The relative standard deviation for the low and high concentration QCs were <6.4% and <3.4%, respectively. The samples analyzed were corrected for dilutions if applicable as well as blanks.

## 2.5. HYSPLIT air mass back trajectory analysis

Air mass back trajectories for each aerosol sample were calculated using NOAA's Hybrid Single-Particle Lagrangian Integrated Trajectory (HYSPLIT; Rolph et al., 2017; Stein et al., 2015). The plugin 'trajstat' (Wang et al., 2009) was used to calculate these trajectories to ultimately aid in the source determination of NH $^{\downarrow}_{+}$ . Utilizing particle dispersion simulation and meteorological data, the model determines the trajectory of an air mass backward in time, starting from a specified point and time. Back trajectories were run at a height of 500 m above ground level every

6 h for the length of the sample collection time as well as four additional days to account of the average lifetime of atmospheric  $NH_X$  (Paulot et al., 2016).

#### 2.6. Potential source contribution function maps

Potential source contribution function (PSCF) maps were created for each season through the combined use of  $\mathrm{NH_4^+}$  concentrations and back trajectory calculations. These maps determine the most likely location of origin of a species (e.g.,  $\mathrm{NH_4^+}$ ) relative to the study site. These calculations are based on the evaluation, for each grid cell (or area), of the ratio of the total number of marked trajectory segment endpoints to the total number of trajectory segment endpoints over that grid cell (Wang et al., 2009).

## 2.7. NH<sub>4</sub> isotope analysis

The determination of  $\delta^{15}$ N-NH<sub>4</sub> follows the protocol of Zhang et al. (2007) based on a coupled off-line wet-chemistry technique involving hypobromite (BrO<sup>-</sup>) oxidation and acetic acid/sodium azide reduction. Only samples with NH<sub>4</sub><sup>+</sup> concentrations greater than 5 µmol were analyzed for isotopic composition due to the high level of uncertainty for lower concentrations (Zhang et al., 2007). Samples above 5 μmol (n = 108) were diluted with ultraclean water (>18 M $\Omega$ ) to either 5  $\mu$ mol-NH<sub>4</sub> or 10 μmol-NH<sub>4</sub>. NH<sub>4</sub> was then oxidized to nitrite (NO<sub>2</sub>) using BrO in an alkaline solution, and further synthesized following the protocol by Zhang et al. (2007). NO<sub>2</sub> concentrations were analyzed to obtain oxidation yields, which were found to completely convert NH<sub>4</sub><sup>+</sup> to NO<sub>2</sub><sup>-</sup> for all samples. The reaction was then stopped by the addition of sodium arsenite to extract the remaining BrO-. Afterward, the samples were transferred into 20 mL vials, crimp-capped with PTFE/butyl septa, and flushed with helium gas for a minimum of 10 min. The NO<sub>2</sub> was then reduced to nitrous oxide gas (N2O) through the addition of 2 mL of 2 M sodium azide buffered in 40% acetic acid solution. After half an hour (minimum), the samples were neutralized using 6 M sodium hydroxide.

Samples were then analyzed for the  $\delta^{15}$ N-N<sub>2</sub>O composition via an automated N<sub>2</sub>O extraction system coupled with a continuous flow Isotope Ratio Mass Spectrometer for determination at m/z 44, 45, and 46. In each sample set, unknowns were calibrated to two internationally recognized NH<sub>4</sub><sup>+</sup> isotopic reference materials, IAEA-N<sub>2</sub> ( $\delta^{15}$ N = 20.4 ‰) and USGS25 ( $\delta^{15}$ N = -30.3 ‰; Böhlke et al., 1993; Böhlke and Coplen, 1995), and an internal QC ( $\delta^{15}$ N = -1.5 ‰) that were run multiple times throughout each run. The isotopic standards underwent the same chemical processing as the unknowns and were used to correct for isotopic fractionation (i.e., from the chemical conversion of NH<sub>4</sub><sup>+</sup> to N<sub>2</sub>O). The isotopic standards had a pooled standard deviation (1 $\sigma$ ) of  $\pm$ 0.6 ‰

for IAEA-N<sub>2</sub> (n = 32),  $\pm 0.8$  % for USGS25 (n = 32), and  $\pm 0.8$  % for the QC (n = 32). Additionally, the pooled standard deviation for duplicates (n = 13 pairs) and replicates (n = 20) was 0.3 % and 0.5 %, respectively.

### 2.8. ISORROPIA-II model analysis

The ISORROPIA-II model performs aerosol thermodynamical equilibrium calculations and can partition  $\mathrm{NH}_x$  between the gas and aerosol phases (Fountoukis and Nenes, 2007). Inputs to the partitioning routine include various elemental and ion concentrations as well as atmospheric temperature and relative humidity. The model was run in the 'reverse' mode under 'metastable' conditions and was done for each sample (n = 81) where all required concentration data were successfully measured (e.g., some samples had limited volume, and not all analyses could be completed). Concentrations for the following elements/ions were inputted:  $\mathrm{Na}^+$ ,  $\mathrm{SO}_4^2^-$ ,  $\mathrm{NH}_4^+$ ,  $\mathrm{NO}_3^-$ ,  $\mathrm{Cl}^-$ ,  $\mathrm{Ca}^{2+}$ ,  $\mathrm{K}^+$ , and  $\mathrm{Mg}^{2+}$ . Additionally, average temperature and relative humidity values, measured during each collection period per sample, were used.

# 2.9. Calculating $\delta^{15}N-NH_{3(q)}$ from aerosol $\delta^{15}N-NH_4^+$

Outputs from ISORROPIA-II and the calculated ion balance of the samples both indicated that the aerosols were essentially completely neutralized by  $NH_{3(g)}$ . Under these conditions, a surplus of  $NH_{3(g)}$  is assumed to stay in the atmosphere, resulting in isotopic fractionation between the aerosol and gas phases (Pan et al., 2018a). To account for this, the  $\delta^{15}N$  values of the original  $NH_{3(g)}$  concentrations were determined using the following isotopic mass-balance model in a well-mixed closed system:

$$\delta_{gas} = \delta_{aerosol} - \epsilon_{aerosol-gas} (1 - f) \tag{1}$$

where  $\delta_{gas}$  is the isotopic composition of the initial  $NH_{3(g)}$ ,  $\delta_{aerosol}$  is the isotopic composition of the final aerosol  $NH_4^+$ , and f is the fraction of the initial  $NH_{3(g)}$  converted to the aerosol  $NH_4^+$ . Epsilon and alpha are related via the following equation:

$$\varepsilon = (\alpha - 1) \times 1000 \tag{2}$$

Therefore, the following formula (Walters et al., 2019) was used to determine  $\delta_{\text{gas}}$ :

$$1000 \ (^{15}\alpha_{NH_4^+(aq)/NH_{3(g)}} - 1) \ (\pm 3.5\%) = 14058 \Big/ T - 12.20 \eqno(3)$$

where T is temperature in Kelvin.

This formula was used for each sample (n = 108), as opposed to a yearly average, to best account for any seasonal differences. To calculate f, concentrations of both  $\mathrm{NH_4^+}$  and  $\mathrm{NH_{3(g)}}$  are needed. Concurrent measurements of  $\mathrm{NH_{3(g)}}$  were not available in this study. Therefore, ISORROPIA-II was used to reproduce gas phase chemistry as well as aerosol evolution during the timeframe of the study.

### 2.10. Stable isotope mixing models in R (SIMMR)

The Bayesian mixing model executed in the R package SIMMR (stable isotopes mixing models in R; Parnell et al., 2013) was implemented. It determines a high number of plausible solutions of source contributions to each sample input by applying Bayes theorem. The model is equipped with a Monte Carlo Markov Chain algorithm that generates plausible solutions for each sources influence on each sample (Parnell et al., 2010, 2013; Cooper et al., 2014). From these *n* realizations, the best estimate (mean) and its uncertainty (standard deviation) can be obtained. SIMMR was used in this study to calculate the likely percentage that each given activity (volatilization/animal waste/fertilizer, industry/fuel combustion, vehicles, marine, biomass burning) was the origin of the NH<sub>3</sub> emissions. Ship emissions in the China region were not included in SIMMR, as the global anthropogenic

emission inventory for NH<sub>3</sub> (1970-2017; McDuffie et al., 2020) shows that off-road/non-road transportation, including ship emissions, comprised less than 1% of the total emissions from 2015 to 2017. Additionally, the δ<sup>15</sup>N-NH<sub>3</sub> signature from ship emissions is currently unknown. Reported values used in SIMMR include: volatilization/animal waste/fertilizer ( $-19.2 \pm 8.3$  %; Freyer, 1978; Heaton, 1987; Frank et al., 2004; Hristov et al., 2009), fuel combustion/industry ( $-15.3 \pm 3.6$  %; Freyer, 1978; Heaton, 1987), vehicle emissions (6.6  $\pm$  2.1 %; Walters et al., 2020; Song et al., 2021), marine sources ( $-6.5 \pm 1.5$  %; Jickells et al., 2003), and biomass burning ( $-6.1 \pm 1.3$  %; Freyer, 1978). The emission source ranges were chosen from sampling methodologies that used active sampling approaches, as it has been documented that passive samplers result in a  $\delta^{15}$ N-NH<sub>3</sub> bias and could potentially be unreliable (Pan et al., 2020; Walters et al., 2020; Kawashima et al., 2021). For the marine signature, we utilize Jickells et al.'s (2003) values associated with aerosol samples collected in remote marine environments, though we note this is also consistent with a marine rainwater study (Altieri et al., 2014). The biomass burning signature is inferred from the ammonium aerosol data in Freyer (1978) who measured the nitrogen in coal that derives from biomass burning. There are no robust actively collected biomass burning signatures for  $\delta^{15}$ N-NH<sub>3</sub>.

# 2.11. Global anthropogenic NH3 emission data retrieval

Anthropogenic NH $_3$  emission data was retrieved from McDuffie et al. (2020) who updated the open-source Community Emissions Data System (CEDS; Hoesly et al., 2019) to develop a new global emission inventory, CEDS<sub>GBD-MAPS</sub> (https://doi.org/10.5281/zenodo.3754964). It contains global anthropogenic emission data of atmospheric pollutants from sector- and fuel-specific sources from 1970 to 2017. Sector sources include agriculture, energy, industry, on road transportation, off road transportation, residential combustion, commercial combustion, other combustion, solvents, waste, and international shipping. Emissions were considered over an area of contribution based on the potential source contribution maps (see results section). This was done for 2015, 2016, and 2017 to calculate the percentage of different anthropogenic sources contributing to the study site.

# 3. Results

## 3.1. Species concentrations

NH $_{+}^{+}$  concentrations varied seasonally (p < 0.05), with a high in winter (2.77  $\pm$  1.06  $\mu g/m^3$ ) and a low in autumn (0.74  $\pm$  0.55  $\mu g/m^3$ ; Fig. 2). Winter had the largest variability, and summer had the least, with autumn and spring being transitions between the two. (Note that blanks were below or near detection limits for N species and were not subtracted from the sample concentrations.).

All measured ions  $(Mg^{2+}, K^+, Na^+, NH_4^+, NO_3^-, Cl^-, SO_4^{2-})$  had the highest average concentrations in the winter except Ca<sup>2+</sup> which was highest in the spring (Table 1; Fig. 3). Additionally, most measured ions  $(Ca^{2+}, Mg^{2+}, K^+, Na^+, Cl^-)$  had the lowest concentrations in the summer except NH<sub>4</sub><sup>+</sup>, NO<sub>3</sub><sup>-</sup>, and SO<sub>4</sub><sup>2-</sup>, which was lowest in the autumn. Overall,  $\mathrm{Mg}^{2+}$  and  $\mathrm{K}^+$  had the lowest average annual concentrations compared to the rest (0.32  $\pm$  0.36  $\mu$ g/m<sup>3</sup> and 0.52  $\pm$  1.10  $\mu$ g/m<sup>3</sup>, respectively), whereas  $NO_3^-$  and  $Na^+$  had the highest annual average concentrations overall (3.82  $\pm$  3.83  $\mu g/m^3$  and 3.40  $\pm$  3.78  $\mu g/m^3$ , respectively). Furthermore, all ions were significantly different amongst seasons (p < 0.05). A majority (>55%) of the  $NO_2^-$  concentrations were at or below detection limit and therefore no  $NO_2^-$  data was included. For field blanks, %N was below the limits of detection; filter blanks were also run for the full suite of ions and chemical species where Ca<sup>2+</sup>, Mg<sup>2+</sup>, and SO<sub>4</sub><sup>2</sup> were found to be <5%. Na<sup>+</sup>, K<sup>+</sup>, and Cl<sup>-</sup> appear to be contaminated as their "blank" values were unreasonably high compared to sample concentrations. Therefore, the samples were not blank-

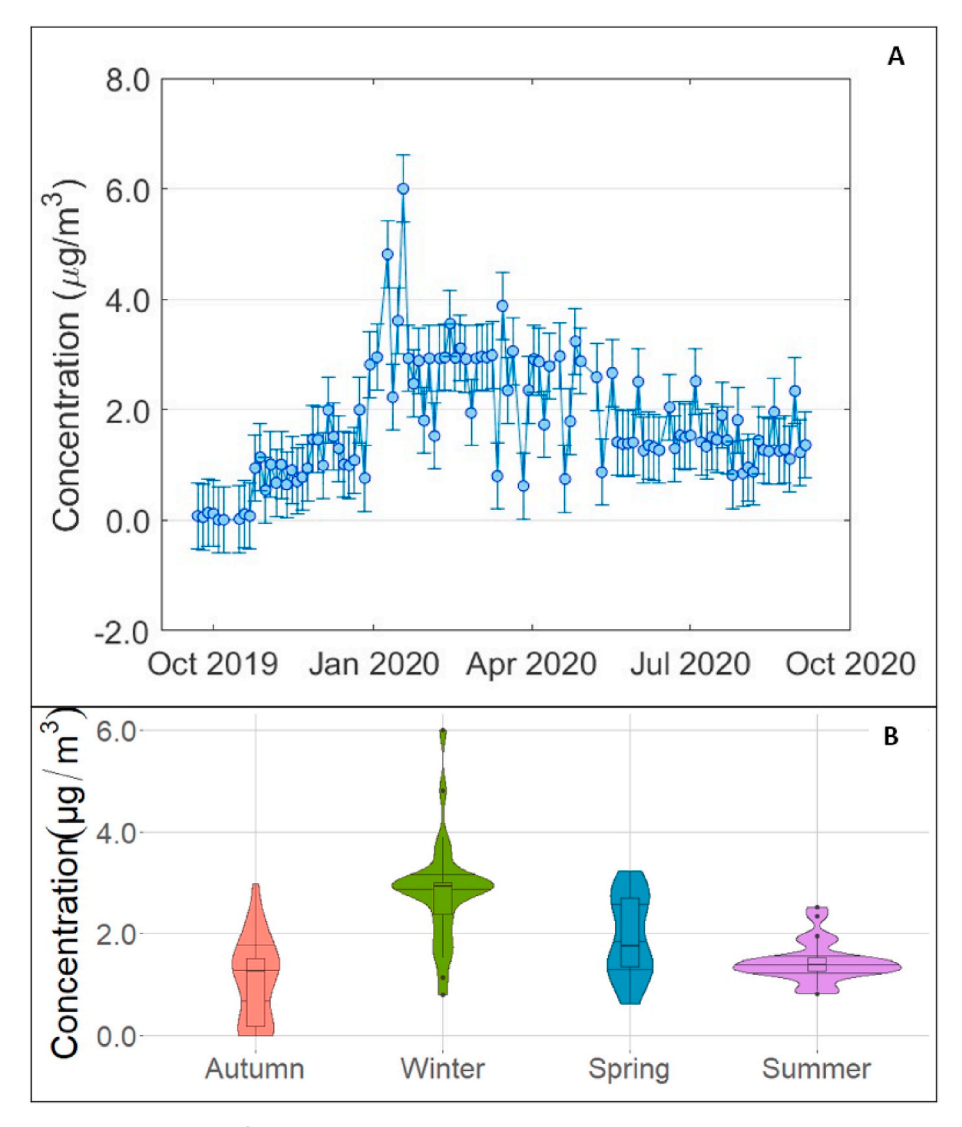


Fig. 2. (A): Time series of  $NH_{+}^{+}$  concentration ( $\mu g/m^{3}$ ). Error bars (A) represent the pooled standard deviation for the concentration measurement technique. (B): Violin plot of  $NH_{+}^{+}$  concentration ( $\mu g/m^{3}$ ) by season (n = 28 (autumn), n = 30 (winter), n = 24 (spring), n = 26 (summer)).

Table 1 Average concentrations  $(\mu g/m^3\pm 1\sigma)$  of measured elements and ions by season and annually.

	Autumn average (μg/m³)	n	Winter average ( $\mu g/m^3$ )	n	Spring average ( $\mu g/m^3$ )	n	Summer average (µg/m³)	n	Annual average (μg/m³)
Ca <sup>2+</sup>	$0.8\pm0.8$	30	$2.5\pm3.3$	31	$2.7\pm2.7$	26	$0.7\pm0.4$	16	$1.8\pm2.5$
$Mg^{2+}$	$0.2\pm0.3$	30	$0.5\pm0.4$	31	$\textbf{0.4} \pm \textbf{0.4}$	26	$0.1\pm0.07$	16	$0.3\pm0.4$
$K^{+}$	$0.2\pm0.2$	30	$1.0\pm1.8$	31	$0.4\pm0.4$	26	$0.2\pm0.1$	16	$0.5\pm1.1$
Na <sup>+</sup>	$1.8\pm2.3$	30	$5.4 \pm 4.2$	31	$4.0 \pm 4.4$	26	$1.4\pm0.6$	16	$3.4\pm3.8$
$NH_4^+$	$0.7\pm0.6$	28	$2.8\pm1.1$	30	$1.9\pm0.8$	24	$1.4\pm0.4$	26	$1.7\pm1.1$
$NO_3^-$	$1.1\pm1.03$	30	$6.2\pm4.5$	31	$5.2\pm4.4$	29	$2.6\pm1.1$	26	$3.8\pm3.8$
Cl-	$2.3\pm3.1$	28	$4.7\pm4.1$	31	$2.4\pm4.5$	26	$0.7\pm0.4$	16	$2.8\pm3.8$
$SO_4^{2-}$	$0.8\pm0.7$	28	$4.1\pm2.9$	31	$3.1\pm2.3$	25	$1.5\pm0.3$	16	$\textbf{2.5} \pm \textbf{2.4}$

#### corrected.

The NH $_4^+$  concentrations found in this study (annual average of 1.7  $\pm$  1.1  $\mu$ g/m $^3$ ; Table 1) are lower compared to Zhang et al. (2013), who studied aerosol NH $_4^+$  concentrations over the Yellow Sea and the East China Sea during autumn. They measured an average of  $4.6 \pm 2.2 \, \mu$ g/m $^3$  over the Northern Yellow Sea and  $3.1 \pm 2.8 \, \mu$ g/m $^3$  over the Southern Yellow Sea and East China Sea. In the open ocean of the Western North Pacific Ocean (as far east as  $\sim$ 140°E, 6°N), Xiao et al. (2018) reported an average NH $_4^+$  concentration of  $0.2 \pm 0.5 \, \mu$ g/m $_3^3$  in aerosol samples during the winter. Compared to our study, these values from Xiao et al. (2018) represent a higher percentage of marine air mass back

trajectories and therefore showed more marine origins.

#### 3.2. Non-sea salt values

Further indicative of terrestrial/anthropogenic inputs is the fraction of non-sea salt (nss) values for various ions. The nss values were calculated based on: nss-X =  $X_{aerosol}$  - (X/Na)<sub>seawater</sub> × Na<sub>aerosol</sub>, where the mass ratios of (X/Na)<sub>seawater</sub> for  $SO_4^-$ ,  $K^+$ ,  $Ca^{2+}$ , and  $Mg^{2+}$  were 0.2515, 0.03701, 0.03821 and 0.012, respectively (Millero, 2006; Nah et al., 2021). All seasons were observed to have nss values > 55%, with the majority >70% (Table 2).

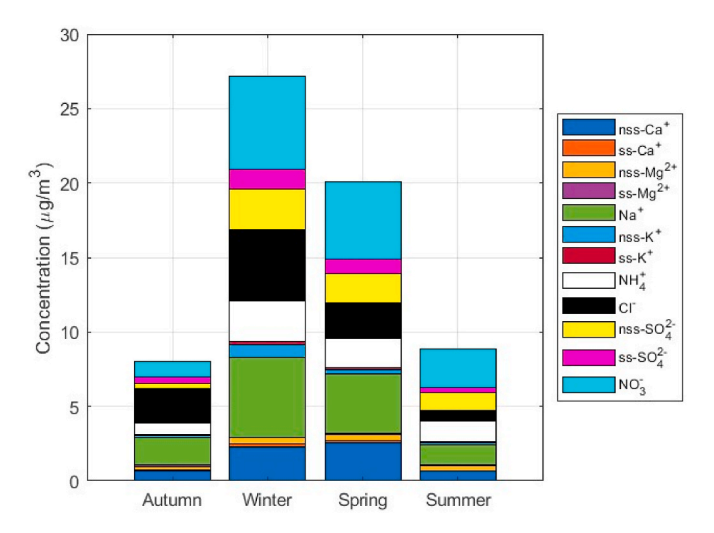


Fig. 3. Stacked bar graph of species concentration changes among the four seasons (autumn, winter, spring, summer).

**Table 2** Average fraction of non-sea salt values (%  $\pm$  1 $\sigma$ ) by season.

	Autumn	Winter	Spring	Summer
	Average (%)	Average (%)	Average (%)	Average (%)
fnss-Ca <sup>2+</sup> fnss-Mg <sup>2+</sup> fnss-K <sup>+</sup> fnss-SO <sub>4</sub> <sup>2-</sup>	$\begin{array}{c} 91.9 \pm 5.4 \\ 90.6 \pm 2.9 \\ 69.0 \pm 15.5 \\ 56.2 \pm 27.2 \end{array}$	$89.8 \pm 6.9 \\ 85.6 \pm 5.0 \\ 70.1 \pm 16.6 \\ 68.6 \pm 13.6$	$\begin{array}{c} 93.7 \pm 4.1 \\ 85.9 \pm 6.0 \\ 68.2 \pm 14.1 \\ 70.8 \pm 16.3 \end{array}$	$92.0 \pm 3.0 \\ 83.6 \pm 5.5 \\ 73.0 \pm 7.2 \\ 78.3 \pm 7.4$

Zhang et al. (2013) measured  $\text{Ca}^{2+}$ ,  $\text{K}^+$ , and  $\text{SO}_4^{2-}$  in Ningbo, China, and calculated their nss values. Higher ratios of nss- $\text{SO}_4^{2-}$ , nss- $\text{K}^+$ , and nss- $\text{Ca}^{2+}$  (all >70%) were detected in fine mode (PM<sub>1,1-2,1</sub>), indicating that most particles originated from terrestrial sources (Zhang et al., 2013). Xiao et al. (2018) analyzed total suspended particulates (e.g., not size-segregated) and also calculated the nss values of  $\text{Ca}^{2+}$ ,  $\text{Mg}^{2+}$ ,  $\text{K}^+$ , and  $\text{SO}_4^{2-}$  during winter in the Western North Pacific Ocean. They found that nss- $\text{Mg}^{2+}$  was only  $13.1 \pm 6.9$ % of the total  $\text{Mg}^{2+}$ , with nss- $\text{Mg}^{2+}$  typically being considered a crustal-derived ion in continental studies (Dueñas et al., 2012; Xiao et al., 2018). Nss- $\text{Ca}^{2+}$  was higher at  $41.8 \pm 17.0$ % whereas the fraction of nss- $\text{SO}_4^{2-}$  comprised 39.7% of total  $\text{SO}_4^{2-}$  in the samples. It was further observed that continental  $\text{SO}_4^{2-}$  can be carried to and impact the open ocean (Xiao et al., 2018).

## 3.3. Species correlations

Pearson correlation values were calculated seasonally between each element and ion (Tables S1A–D) to investigate crustal versus marine sources. For all four seasons, Na $^+$  and Cl $^-$ , Na $^+$  and ss-SO $_4^2$ , and Mg $^{2+}$  (ss- and nss-) and ss-SO $_4^2$  were strongly positively correlated (R  $\geq$  0.70). Na $^+$  and Mg $^{2+}$  (ss- and nss-) were also strongly positively correlated during each season (R > 0.85), as well as Cl $^-$  and ss-Mg $^{2+}$  (R  $\geq$  0.70). Furthermore, Cl $^-$  and ss-SO $_4^2$  were strongly positively correlated for each season (R > 0.70). Overall, these strong relationships are not surprising, as they are ions derived from sea salt. Nss-K $^+$ , nss-Ca $^{2+}$  and nss-Mg $^{2+}$  also are moderately or strongly correlated throughout the seasons (Tables S1A–D), which are indicative of crustal (terrestrial) sources (Dueñas et al.,2012; Xiao et al., 2013, 2017, 2018).

When looking at the nitrogen species,  $NH_4^+$  and  $NO_3^-$  both had a strong correlation with nss- $SO_4^{2^-}$  in autumn (R>0.65; Table S1A). Moderate correlations in autumn include  $NH_4^+$  and nss- $Ca^{2^+}$  (R=0.45) as well as  $NO_3^-$  with  $Ca^{2^+}$  (ss- and nss-),  $Mg^{2^+}$  (ss- and nss-),  $Na^+$ ,  $Cl^-$ , and  $NH_4^+$  (R>0.40; Table S1A). No strong or moderate correlations were observed in winter, except  $NO_3^-$  and nss-  $Ca^{2^+}$  (R=0.41;

Table S1B).  $NH_4^+$  and  $NO_3^-$  were strongly correlated in the spring (R=0.62, Table S1C), and  $NH_4^+$  was moderately correlated with nss-SO $_2^{2^-}$  (R=0.43; Table S1C). The summer season is interesting due to the negative correlations observed that are not present in the other seasons.  $NH_4^+$  was strongly negatively correlated with ss-Ca $^{2+}$ ,  $Mg^{2+}$  (ss- and nss-), ss-SO $_4^{2^-}$ , ss-K $^+$  and Na $^+$  (R>-0.60; Table S1D). Moderate correlations include  $NH_4^+$  with nss-Ca $^{2+}$ , nss-K $^+$ , and Cl $^-$  (R>-0.40). Additionally,  $NO_3^-$  was moderately negatively correlated with ss-K $^+$ , ss-SO $_4^{2^-}$ , ss-Ca $^{2+}$ , ss-Mg $^{2+}$ , Na $^+$ , and Cl $^-$  (R=-0.56 to -0.59; Table S1D).

 $\delta^{15} N-N H_4^+$  values were also checked for potential correlations between the measured species. During autumn,  $\delta^{15} N-N H_4^+$  was strongly negatively correlated with nss-SO<sub>2</sub>-( (R = -0.63) and NH<sub>4</sub>+ concentration (R = -0.67), and moderately negatively correlated with NO<sub>3</sub>-(R = -0.47). For every season besides autumn,  $\delta^{15} N-N H_4^+$  remained moderately or strongly correlated with nss-Ca<sup>2+</sup> (R > 0.50). For example, in Spring,  $\delta^{15} N-N H_4^+$  was moderately positively correlated with nss-Ca<sup>2+</sup> (R = 0.52) and moderately negatively correlated with NH<sub>4</sub>+ (R = -0.54). In summer,  $\delta^{15} N-N H_4^+$  was strongly positively correlated with Na<sup>+</sup> and Cl<sup>-</sup> (R > 0.60) and negatively correlated with NO<sub>3</sub>-(R = -0.65).

## 3.4. Air mass back trajectories

Although seasonally different, the air mass origins of the aerosol samples were predominantly continental (Fig. S1A-D). For autumn, winter, and spring, the air masses were continental in origin, with both medium and long-range transport and a majority coming from the Northwest (Fig. S1A-C). During the summer, a fraction of the air masses came from the marine system, with the remaining from the continent, both as medium and long-range transportation (Fig. S1D).

The air mass back trajectories and concentration data were further used to create potential source contribution function (PSCF) maps per season (Fig. 4A–D). The PSCF analysis shows that for all four seasons, the primary source region for  $NH_3$  is fairly local to the study site, with autumn (Fig. 4A) and summer (Fig. 4D) showing a larger geographical footprint.

## 3.5. Observed NH<sub>4</sub> isotopes

The NH $_4^+$  isotope values fall in the range of -10.4~% to 39.7% (Fig. 5A). Very small variability is present in autumn but increases with the remaining seasons, with the largest in winter (Fig. 5B). NH $_4^+$  isotope values were different seasonally (p < 0.05), with higher average values in spring (13.3  $\pm$  7.9 %) and summer (15.6  $\pm$  6.2 %) compared to autumn (3.2  $\pm$  2.5 %) and winter (3.8  $\pm$  11.4 %).

As stated, autumn has minimal variation compared to the other seasons. This could be due to the different sampling periods, as the aerosol samples in autumn were collected for 72 h, whereas in the other seasons collection periods were either 48 or 24 h. The shorter sampling periods are likely the cause for increased variation.

### 3.6. Calculated $NH_{3(g)}$ isotopes

Based on ISORROPIA-II, excess NH<sub>3(g)</sub> was always present (n = 81), which is comparable to Nenes et al. (2021) who discusses the recent buildup of NH<sub>3(g)</sub> in China. Additionally, pH was calculated to fall between 6 and 8, which is consistent with a system that has a surplus of NH<sub>3(g)</sub>. Given the excess of NH<sub>3(g)</sub>, the influence of equilibrium isotopic fractionation on NH<sub>4</sub><sup>+</sup> is large. Seasonally, the average fractionation ( $\varepsilon$ ; see eqs. (1) and (3)) was 37.4  $\pm$  1.1 for autumn, 38.9  $\pm$  0.8 for winter, 36.9  $\pm$  0.9 for spring, and 35.4  $\pm$  0.4 for summer. Calculated NH<sub>3(g)</sub> isotope values were different seasonally (p < 0.05) with higher values in summer ( $-19.7 \pm 6.3$  %) and spring ( $-23.7 \pm 8.3$  %) compared to winter ( $-35.2 \pm 11.6$  %) and autumn ( $-34.3 \pm 3.4$  %). However, individually calculated  $\varepsilon$  values were subtracted from each sample (e.g., not the seasonal average).

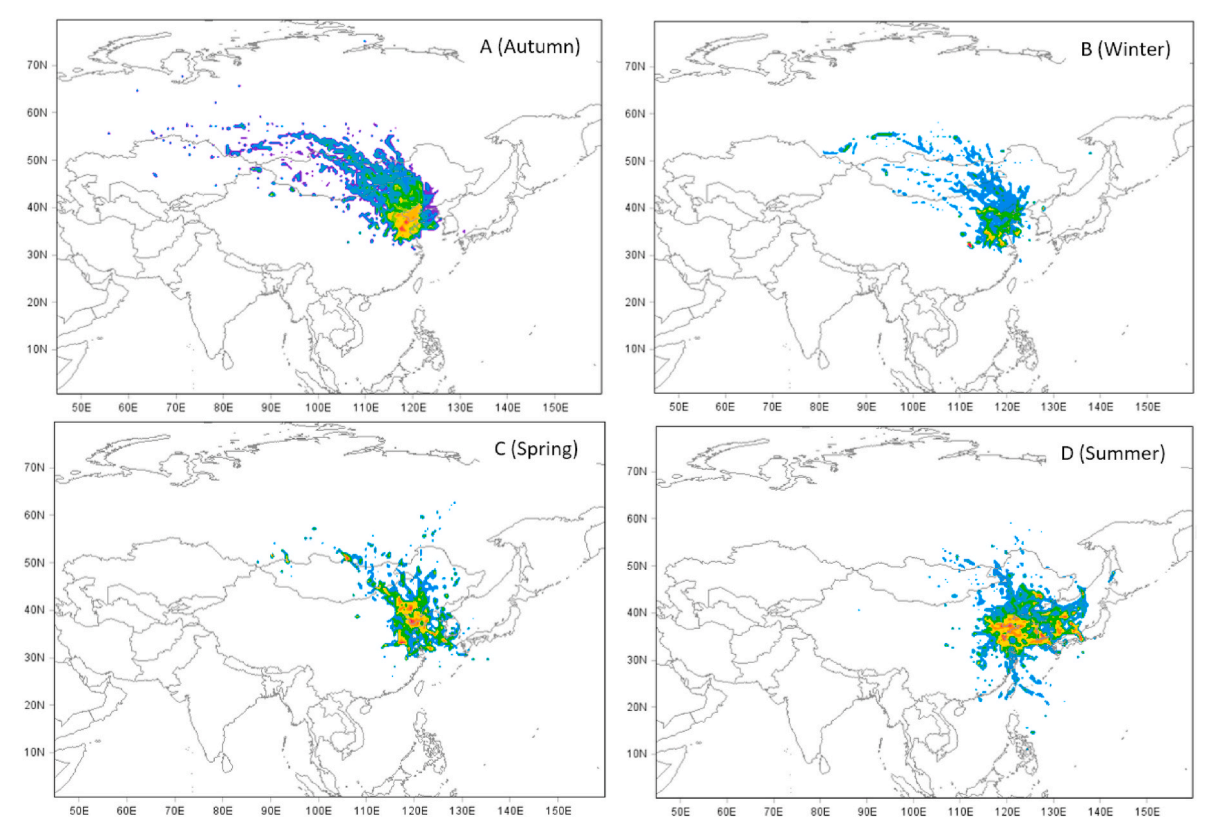


Fig. 4. Potential source contribution function analysis by season (A = Autumn, B = Winter, C = Spring, D = Summer), with warmer colors (red, orange, yellow) representing greater relative impact of source locations versus cooler colors (green, blue, purple) representing lower relative contributions to the measured ammonium concentrations at Changdao Island.

### 3.7. Isotope mixing model results

Based on SIMMR,  $NH_{3(g)}$  from agriculture was consistently the greatest source contribution in each season (all >65 %; Fig. 6), with a maximum in the summer, and minimum in winter. Industrial fuel combustion was consistently the second highest source, with a maximum in winter, and minimum in summer. The remaining sources were all <10 % individually for all seasons.

#### 4. Discussion

NH<sub>4</sub> is an alkaline species known for forming haze, with the Northern China Plain (in close proximity to the current study site) being one of the greatest atmospherically polluted regions in China (NH3, sulfuric acid, nitric acid, ammonium sulfate, ammonium hydrogen sulfate, etc; Xiang et al., 2022). During the 2020 expanded Chinese Lunar New Year celebration (January 24 to February 10), China was in a never-before-seen state of shutdown, due to the majority of people being contained in their homes to limit the spread of the novel coronavirus disease (COVID-19, Chang et al., 2020). Yet, widespread haze pollution still arose over Eastern China during this time (Chang et al., 2020). This time period overlapped with the current study, where NH<sub>4</sub><sup>+</sup> concentrations were highest in the winter, supporting the strong relationship between NH<sup>+</sup> and haze formation and most likely explaining the winter maximum in the dataset. Additionally, the higher NO<sub>3</sub> and SO<sub>4</sub><sup>2-</sup> concentrations also found in winter (Fig. 3) will favor more NH<sub>(D)</sub> formation relative to NH<sub>3(g)</sub> (Seinfeld and Pandis, 2016). Overall, our observations of the particulate matter exported to the ocean largely supports crustal/anthropogenic origins (species concentrations in Table 1, nss calculations in Table 2, and species correlations in Tables S1A-D).

The average  $\delta^{15}N-NH_4^+$  (and calculated  $\delta^{15}N-NH_3$ ) values were lowest in the winter (Fig. 5) due to the high number of negative values

present. Overall, the seasonal changes in the  $\delta^{15}N$  values were not explained by changes in chemistry or the partitioning of NH<sub>3</sub>/NH<sub>4</sub><sup>+</sup>, based on the fractionation calculations and neutralization ratios (ISO-RROPIA output). These wintertime measurements roughly overlap with the COVID-19 lockdown in China, although different regions enacted different restrictive measures based on the number of cases in the area (Chen et al., 2020). It is suggested that agricultural activities did not slow down dramatically, but vehicles (including public transportation) greatly decreased and there was a slight reduction in industrial production (Chen et al., 2020), potentially explaining the lower  $\delta^{15}N$  in the winter compared to other seasons since vehicles are the only positive  $\delta^{15}N$ -NH<sub>3</sub> source. Therefore, one might expect in a different year, with no lockdown, that vehicles might be a greater contributor than observed in this study.

The SIMMR model results (Fig. 6) predict a dominant signal from agricultural emissions (including volatilization, animal husbandry and use of fertilizers), however, the similarity in the isotopic ranges for industry and agriculture mean that these two sources are both strong levers on the predicted probability in a way that can be difficult to distinguish using this modeling technique. Marine and biomass burning also have similar ranges, which the model cannot separate well. However, marine sources and biomass burning are shown to have minimal impact on our study site, both indicated by SIMMR as well as other tools used in this study (correlation tests, emission inventories, etc). Therefore, even though SIMMR cannot separate these two sources well, we are confident they are not major contributors to our site. This mixing model approach also does not consider changes in physical drivers of ammonia dynamics such as seasonal weather, soil pH, land/water type, etc. Still, several lines of evidence support agricultural emissions as an important driver of the NH<sub>4</sub> signals, particularly during our collection period.

He et al. (2021) implemented a machine learning technique to assess the effect of the Spring Festival and COVID-19 on NH<sub>3</sub> emissions in the

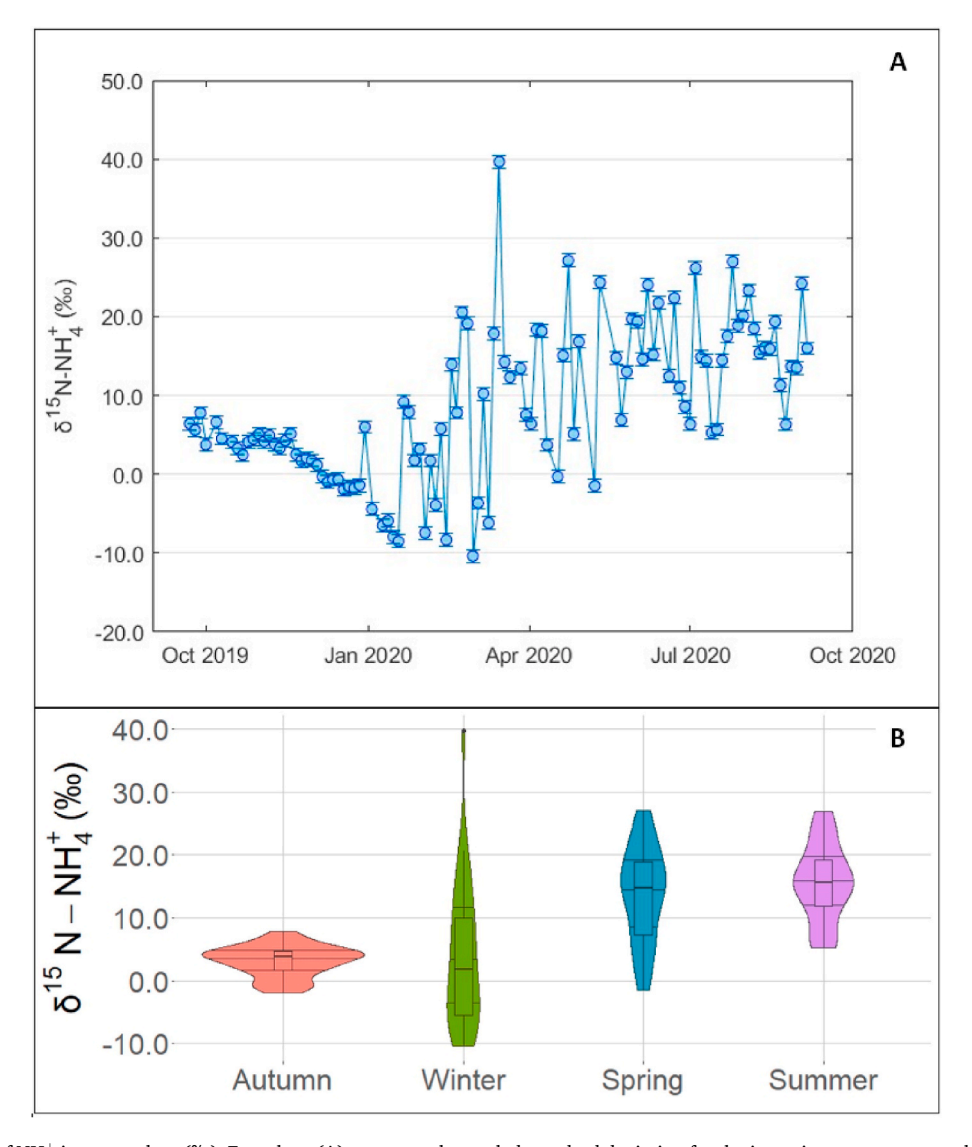
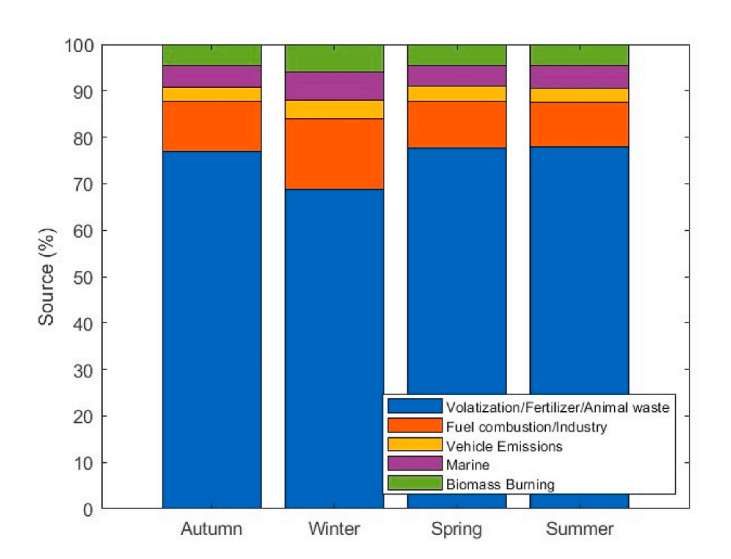


Fig. 5. (A): Time series of  $NH_4^+$  isotope values (‰). Error bars (A) represent the pooled standard deviation for the isotopic measurement technique. (B): Violin plot of  $NH_4^+$  isotope values (‰) by season (n = 28 (autumn), n = 29 (winter), n = 25 (spring), n = 26 (summer)).



**Fig. 6.** Stacked bar graph of probable NH<sub>3</sub> source contributions among the four seasons (calculated by SIMMR).

North China Plain, where they estimated a larger decrease in NH $_3$  concentrations in urban areas compared to rural areas. Xu et al. (2022) studied changes in NH $_3$  due to the lockdown enforcements in China, where they used surface NH $_3$  measurements, satellite NH $_3$  observations, and GEOS-Chem simulations. Contrasting with He et al. (2021), Xu et al. (2022) reported an overall rise in NH $_3$  emissions, but with the increase being most distinct at rural sites, where concentrations were higher during COVID-19 in 2020 than the equivalent periods in earlier years. Specifically in northern China, the NH $_3$  increase is thought to be mainly driven by increased agricultural practices. Overall, the Chen et al. (2020), He et al. (2021), and Xu et al. (2022) studies lend support for decreased emissions from vehicles and industry relative to agricultural activities, including animal husbandry.

To test the sensitivity of the SIMMR results, which were dependent on the extent of fractionation factors calculated using the predicted ISORROPIA [NH $_3$ ] gas outputs from ISORROPIA-II, we changed the fraction of [NH $_3$ ] (and therefore the fractionation) by 10 %, 20 % and 30 %. This changed the  $\delta^{15}$ N–NH $_3$  that was then input into SIMMR. Even with a 20 % error in fractionation, agricultural activities were still the dominant source in all seasons. Only with a 30 % change in fractionation did we see an important change in results, with industry becoming a larger source contribution than agriculture in summer. While

uncertainties in both the ISORROPIA-II results and SIMMR results remain, overall the sensitivity tests build confidence in the hypothesis that agricultural activities dominate NH<sub>4</sub><sup>+</sup> in the region.

Several additional lines of evidence support the importance of agriculture/agricultural emissions. Eastern China, near the study site, is a mix of farmland and urban areas. Pan et al. (2018b) identified different NH $_3$  hotspots (>1 µg/m $^3$ ) in this area based upon a year-round observational network, utilizing a passive NH $_3$  monitoring network based on a diffusive technique with monthly integrated measurements at 53 locations. They considered the connections between hot spots and six different types of land use: desert, farmland, grassland, mountain and forest, urban, and waterbody. When comparing the PSCF (Fig. 4A–D) results from this study to the hotspots identified by Pan et al. (2018b) by season, we find that autumn and spring are most heavily influenced by farmlands, winter is a mix of farmlands and urban areas, and while summer overlaps with farmlands as well, it is the only season that includes noticeable transport from the ocean. (Note that airmasses from the ocean do not have to carry significant marine-based NH $_4^+$ ).

The majority of the aerosol composition of the samples is sourced from nss derived ions (Tables S1A-D), therefore, the marine air masses observed in the summer likely explain the lower concentrations seen during this season (Table 1). This is additionally consistent with the CEDS<sub>GBD-MAPS</sub> emissions inventory, which also identifies agriculture (non-combustion sources only (e.g., excludes open fires)) as the main NH<sub>3</sub> emission source to this region. For the years 2015-2017, agricultural activities comprised roughly 77.3  $\pm$  0.2 % of NH $_3$  emissions on an annual basis, with the greatest contributions observed in spring (86.4  $\pm$ 0.1 %). The wintertime emissions inventory only calculated a contribution of 51.2  $\pm$  0.4 % from agricultural emissions, which may be underestimated based on the isotopic results of the current study, which suggests agriculture accounts for roughly 65 % of the NH3 emissions in winter (Fig. 6). However, it is possible that the discrepancy in these values stems from the timing of the current study, during the COVID-19 lockdown, which resulted in a decrease in transportation activities, and could have therefore resulted in a higher agricultural signal compared to other years.

The Yellow Sea is bordered by the three peninsulas (Liaodong, Shandong, and Korea), all well populated and industrialized, making the Northern Yellow Sea vulnerable to anthropogenic input, which dominates based on the ion budgets year-round (e.g., nss values for the measured species are always >55 % (Table 2)). This is further supported by the calculated air mass back trajectories, in which the majority of samples originated from the continent (Fig. S1A-D). The PSCF analysis (Fig. 4A-D), SIMMR results (Fig. 6), and the CEDS<sub>GBD-MAPS</sub> emissions inventory support agriculture as the primary source contribution compared to other potential sources.

## 5. Conclusion

Conflicts in the literature reveal uncertainty regarding source origins of N deposited to the open ocean, making it difficult to determine continental/anthropogenic or marine/natural sources as the dominant input. This study aims to help bridge that gap in understanding by quantifying the influence of anthropogenic emissions of reactive N on the atmospheric composition of aerosols and sources of aerosol  $NH_4^+$ , with a focus on seasonal trends.

Strong seasonal trends (p<0.05) were found in the aerosol composition as well as the  $\delta^{15}N-NH_{+}^{+}$  and  $\delta^{15}N-NH_{3(g)}$  values.  $NH_{+}^{+}$  concentrations varied with a high in winter ( $2.83\pm1.1~\mu g/m^{3}$ ) and low in autumn ( $0.7\pm0.6~\mu g/m^{3}$ ). The other measured elements and ions ( $Mg^{2+}$ ,  $K^{+}$ ,  $Na^{+}$ ,  $NH_{+}^{+}$ ,  $NO_{3}^{-}$ ,  $Cl^{-}$ ,  $SO_{4}^{2-}$ ) also had the highest concentrations in the winter except  $Ca^{2+}$ , which was highest in the spring. Additionally, other measured elements and ions ( $Ca^{2+}$ ,  $Mg^{2+}$ ,  $K^{+}$ ,  $Na^{+}$ ,  $Cl^{-}$ ) had the lowest concentrations in the summer except  $NO_{3}^{-}$ , and  $SO_{4}^{2-}$  which were lowest in the autumn. Furthermore, the annual fraction of nss values for  $Ca^{2+}$ ,  $Mg^{2+}$ ,  $K^{+}$ , and  $SO_{4}^{2-}$  were all high (>65 %).

 $\delta^{15} N-NH_+^4$  had higher values in spring (13.3  $\pm$  7.9 %) and summer (15.6  $\pm$  6.2 %) compared to autumn (3.2  $\pm$  2.5 %) and winter (3.8  $\pm$  11.4 %). Calculated NH3(g) isotope values also had higher values in summer (–19.7  $\pm$  6.3 %) and spring (–23.67  $\pm$  8.3 %) compared to winter (–35.2  $\pm$  11.6 %) and autumn (–34.3  $\pm$  3.4 %). This data, together with the air mass back trajectories, provide evidence for continental origins of NH $_+^4$  deposition primarily as a result of anthropogenic agricultural activities (volatilization/animal waste/fertilizer) throughout the year. Given the anthropogenic origin of NH $_+^4$  and its bioavailability, the results from this study should be further interpreted within the context of total inorganic and organic wet and dry N deposition to the NPO. It is crucial to bridge the gap in understanding of the impact of anthropogenic and marine sources on reactive N deposition to better determine the drivers of biogeochemical changes in the open ocean.

#### CRediT authorship contribution statement

Alexandra B. MacFarland: Investigation, sample analyses/interpretation, Writing – original draft. Emily E. Joyce: Investigation, sample analyses/processing, Writing – review & editing. Xuchen Wang: Conceptualization, Investigation, sample collection/processing. Wendell W. Walters: Conceptualization, interpretation, Writing – review & editing. Katye E. Altieri: interpretation, Writing – review & editing. Hayley N. Schiebel: Conceptualization, Funding acquisition. Meredith G. Hastings: Conceptualization, interpretation, Supervision, Writing – review & editing, Funding acquisition.

#### **Declaration of competing interest**

The authors declare the following financial interests/personal relationships which may be considered as potential competing interests: Meredith Hastings reports financial support was provided by National Science Foundation.

# Data availability

The link is shared at the end of the manuscript under "data availability"

# Acknowledgements

This research was funded by the National Science Foundation (NSF-OCE #1851343). Additionally, the authors thank Joe Orchardo at Brown University for his aid in running the ICP as well as Ruby Ho (lab manager for the Hastings lab) for instrumental support.

# Appendix A. Supplementary data

Supplementary data to this article can be found online at https://doi.org/10.1016/j.atmosenv.2023.120034.

#### References

Altieri, K.E., Fawcett, S.E., Hastings, M.G., 2021. Reactive nitrogen cycling in the atmosphere and ocean. Annual Reviews 49, 523–550.

Altieri, K.E., Fawcett, S.E., Peters, A.J., Sigman, D.M., Hastings, M.G., 2016. Marine biogenic source of atmospheric organic nitrogen in the subtropical North Atlantic. Proc. Natl. Acad. Sci. USA 113 (4), 925–930.

Altieri, K.E., Hastings, M.G., Gobel, A.R., Peters, A.J., Sigman, D.M., 2013. Isotopic composition of rainwater nitrate at Bermuda: the influence of air mass source and chemistry in the marine boundary layer. J. Geophys. Res. Atmos. 118 (19).

Altieri, K.E., Hastings, M.G., Peters, A.J., Oleynik, S., Sigman, D.M., 2014. Isotopic evidence for a marine ammonium source in rainwater at Bermuda. Global Biogeochem. Cycles 28 (10), 1066–1080.

Böhlke, J.K., Coplen, T.B., 1995. Interlaboratory comparison of reference materials for nitrogen-isotope-ratio measurements, reference and intercomparison materials for stable isotopes of light elements. In: Proceedings of the IAEA- TECDOC-825 Consultants Meeting, vol. 1993. Vienna, Austria.

Böhlke, J.K., Gwinn, C.J., Coplen, T.B., 1993. New reference materials for nitrogenisotope- ratio measurements. Geostand. Geoanal. Res. 17, 159–164.

- Chang, Y., Huang, R.-J., Ge, X., Huang, X., Hu, J., Duan, Y., Zou, Z., Liu, X., Lehmann, F., 2020. Puzzling haze events in China during the coronavirus (COVID-19) shutdown. Geophys. Res. Lett. 47.
- Chen, H., Huo, J., Fu, Q., Duan, Y., Xiao, H., Chen, J., 2020. Impact of quarantine measures on chemical compositions of PM2.5 during the COVID-19 epidemic in Shanghai, China. Sci. Total Environ. 743.
- Cooper, R.J., Krueger, T., Hiscock, K.M., Rawlins, B.G., 2014. Sensitivity of fluvial sediment source apportionment to mixing model assumptions: a Bayesian model comparison. Water Resour. Res. 50, 9031–9047.
- Cornell, S.E., Jickells, T.D., Cape, J.N., Rowland, A.P., Duce, R.A., 2003. Organic nitrogen deposition on land and coastal environments: a review of methods and data. Atmos. Environ. 37 (16), 2173–2191.
- Duce, R.A., LaRoche, J., Altieri, K., Arrigo, K.R., Baker, A.R., Capone, D.G., Cornell, S., et al., 2008. Impacts of atmospheric anthropogenic nitrogen on the open ocean. Science 320 (5878), 893–897.
- Dueñas, C., Fernández, M.C., Gordo, E., Cañete, S., Pérez, M., 2012. Chemical and radioactive composition of bulk deposition in Málaga (Spain). Atmos. Environ. 62, 1–8.
- Elser, J., Andersen, T., Baron, J., Bergstrom, A.-K., Jansson, M., Kyle, M., Nydick, K., Steger, L., Hessen, D., 2009. Shifts in lake N:P stoichiometry and nutrient limitation driven by .atmospheric nitrogen deposition. Science 326 (5954), 835–837.
- Fountoukis, C., Nenes, A., 2007. Isorropia II: a computationally efficient thermodynamic equilibrium model for K+-Ca2+-Mg2+-NH+4-Na+-SO2-4-NO-3-Cl--H2O aerosols. Atmos. Chem. Phys. 7, 4639-4659.
- Frank, D.A., Evans, R.D., Tracy, B.F., 2004. The role of ammonia volatilization in controlling the natural 15N abundance of a grazed grassland. Biogeochemistry 68, 169–178.
- Freyer, H.D., 1978. Seasonal trends of NH4+ and NO3- nitrogen isotope composition in rain collected at Jülich, Germany. Tellus 30, 83-92.
- Galloway, J.N., Dentener, F.J., Capone, D.G., Boyer, E.W., Howarth, R.W., Seitzinger, S. P., Asner, G.P., et al., 2004. Nitrogen cycles: past, present, and future. Biogeochemistry 70 (2), 153–226.
- Galloway, J.N., Keene, W.C., Artz, R.S., Miller, J.M., Church, T.M., Knap, A.H., 1989. Processes controlling the concentrations of SO4=, NO3-, NH4+, H+, HCOOT and CH3COOT in precipitation on Bermuda. Tellus B 41B (4), 427–443.
- Galloway, J.N., Keene, W.C., Likens, G.E., 1996. Processes controlling the composition of precipitation at a remote southern hemispheric location: torres del Paine National Park, Chile. J. Geophys. Res. 101 (D3), 6883–6897.
- Galloway, J.N., Likens, G.E., Keene, W.C., Miller, J.M., 1982. The composition of precipitation in remote areas of the world. J. Geophys. Res. 87 (NC11), 8771–8786.
- Gobel, A.R., Altieri, K.E., Peters, A.J., Hastings, M.G., Sigman, D.M., 2013. Insights into anthropogenic nitrogen deposition to the North Atlantic investigated using the isotopic composition of aerosol and rainwater nitrate. Geophys. Res. Lett. 40 (22), 5977–5982.
- Gruber, N., Sarmiento, J.L., 1997. Global patterns of marine nitrogen fixation and denitrification. Global Biogeochem. Cycles 11 (2), 235–266.
- Heaton, T.H.E., 1987. 15N14N ratios of nitrate and ammonium in rain at Pretoria, South Africa. Atmos. Environ. 21, 843–852.
- He, Y., Pan, Y., Gu, M., Sun, Q., Zhang, Q., Zhang, R., Wang, Y., 2021. Changes of ammonia concentrations in wintertime on the North China Plain from 2018 to 2020. Atmos. Res. 253, 105490.
- Hoesly, R., O'Rourke, P., Braun, C., Feng, L., Smith, S.J., Pitkanen, T., Siebert, J., Vu, L., Presley, M., Bolt, R., Goldstein, B., Kholod, N., 2019. CEDS: Community Emissions Data System (Version Dec-23-2019), Zenodo.
- Hristov, A.N., Zaman, S., Vander Pol, M., Ndegwa, P., Campbell, L., Silva, S., 2009. Nitrogen losses from dairy manure estimated through nitrogen mass balance and chemical markers. J. Environ. Qual. 38, 2438–2448.
- Jickells, T.D., Buitenhuis, E., Altieri, K., Baker, A.R., Capone, D., Duce, R.A., Dentener, F., et al., 2017. A reevaluation of the magnitude and impacts of anthropogenic atmospheric nitrogen inputs on the ocean. Global Biogeochem. Cycles 31 (2), 289–305.
- Jickells, T.D., Kelly, S.D., Baker, A.R., Biswas, K., Dennis, P.F., Spokes, L.J., Witt, M., Yeatman, S.G., 2003. Isotopic evidence for a marine ammonia source. Geophys. Res. Lett. 30 (7).
- Johnson, K.S., Riser, S.C., Karl, D.M., 2010. Nitrate supply from deep to near-surface waters of the North Pacific subtropical gyre. Nature 465 (7301), 1062–1065.
- Karl, D.M., Church, M.J., Dore, J.E., Letelier, R.M., Mahaffey, C., 2012. Predictable and efficient carbon sequestration in the North Pacific Ocean supported by symbiotic nitrogen fixation. Proc. Natl. Acad. Sci. USA 109 (6), 1842–1849.
- Kawashima, H., Ogata, R., Gunji, T., 2021. Laboratory-based validation of a passive sampler for determination of the nitrogen stable isotope ratio of ammonia gas. Atmos. Environ. 245, 118009.
- Kim, I.-N., Lee, K., Gruber, N., Karl, D.M., Bullister, J.L., Yang, S., Kim, T.-W., 2014. Increasing anthropogenic nitrogen in the North Pacific ocean. Science 346 (6213), 1102–1106.
- Kim, T.W., Lee, K., Najjar, R.G., Jeong, H.D., Jeong, H.J., 2011. Increasing N abundance in the northwestern Pacific Ocean due to atmospheric nitrogen deposition. Science 334 (6055), 505–509.
- Knapp, A.N., Hastings, M.G., Sigman, D.M., Lipschultz, F., Galloway, J.N., 2010. The flux and isotopic composition of reduced and total nitrogen in Bermuda rain. Mar. Chem. 120 (1), 83–89.
- Kurokawa, J., Ohara, T., Morikawa, T., Hanayama, S., Janssens- Maenhout, G., Fukui, T., Kawashima, K., Akimoto, H., 2013. Emissions of air pollutants and greenhouse gases over Asian regions during 2000–2008: regional Emission inventory in Asia (REAS) version 2. Atmos. Chem. Phys. 13, 11019–11058.

- Letscher, R.T., Primeau, F., Moore, J.K., 2016. Nutrient budgets in the subtropical ocean gyres dominated by lateral transport. Nat. Geosci. 9 (11), 815–819.
- Luo, X.S., Tang, A.H., Shi, K., Wu, L.H., Li, W.Q., Shi, W.Q., Shi, X.K., Erisman, J.W., Zhang, F.S., Liu, X.J., 2014. Chinese coastal seas are facing heavy atmospheric nitrogen deposition. Environ. Res. Lett. 9, 095007.
- McDuffie, E.E., Smith, S.J., O'Rourke, P., Tibrewal, K., Venkataraman, C., Marais, E.A., Zheng, B., Crippa, M., Brauer, M., Martin, R.V., 2020. A global anthropogenic emission inventory of atmospheric pollutants from sector- and fuel-specific sources (1970–2017): an application of the Community Emissions Data System (CEDS). Earth Syst. Sci. Data 12, 3413–3442.
- Millero, F.J., 2006. Chemical Oceanography, third ed. CRC Press, p. 496.
- Nah, T., Yang, J., Wang, J., Sullivan, A.P., Weber, R.J., 2021. Fine aerosol acidity and water during summer in the eastern North Atlantic. Atmosphere 12 (1040).
- Nenes, A., Pandis, S.N., Kanakidou, M., Russell, A.G., Song, S., Vasilakos, P., Weber, R.J., 2021. Aerosol acidity and liquid water content regulate the dry deposition of inorganic reactive nitrogen. Atmos. Chem. Phys. 21, 6023–6033.
- O'Dell, J.W., 1993. In: Method 350.1, Revision 2.0: Determination of Ammonia Nitrogen by Semi-automated Colorimetry. US EPA
- Pan, Y., Tian, S., Liu, D., Fang, Y., Zhu, X., Gao, M., Gao, J., Michalski, G., Wang, Y., 2018a. Isotopic evidence for enhanced fossil fuel sources of aerosol ammonium in the urban atmosphere. Environ. Pollut. 238, 942–947.
- Pan, Y., Gu, M., Song, L., Tian, S., Wu, D., Walters, W.W., Yu, X., Lü, X., Ni, X., Wang, Y., 2020. Systematic low bias of passive samplers in characterizing nitrogen isotopic com- position of atmospheric ammonia. Atmos. Res. 243, 105018.
- Pan, Y., Tian, S., Zhao, Y., Zhang, L., Zhu, X., Gao, J., Huang, W., Zhou, Y., Song, Y., Zhang, Q., Wang, Y., 2018b. Identifying ammonia hotspots in China using a national observation network. Environ. Sci. Technol. 52, 3926–3934.
- Parnell, A.C., Inger, R., Bearhop, S., Jackson, A.L., 2010. Source partitioning using stable isotopes: coping with too much variation. PLoS One (5), 1–6.
- Parnell, A.C., Phillips, D.L., Bearhop, S., Semmens, B.X., Ward, E.J., Moore, J.W., Jackson, A.L., Grey, J., Kelly, D.J., Inger, R., 2013. Bayesian stable isotope mixing models. Environmetrics 24 (6), 387–399.
- Paulot, F., Ginoux, P., Cooke, W.F., Donner, L.J., Fan, S., Lin, M.-Y., Mao, J., Naik, V., Horowitz, L.W., 2016. Sensitivity of nitrate aerosols to ammonia emissions and to nitrate chemistry: implications for present and future nitrate optical depth. Atmos. Chem. Phys. 16, 1459–1477.
- Quay, P., Peacock, C., Bjorkman, K., Karl, D., 2010. Measuring primary production rates in the ocean: enigmatic results between incubation and non-incubation methods at Station ALOHA. Global Biogeochem. Cycles 24 (3).
- Ren, P., Luo, C., Zhang, H., Schiebel, H., Hastings, M.G., Wang, X., 2022. Atmospheric particles are major sources of aged anthropogenic organic carbon in marginal seas. Environ. Sci. Technol. 56, 14198–14207.
- Rolph, G., Stein, A., Stunder, B., 2017. Real-time environmental applications and display system: READY. Environ. Model. Software 95, 210–228.
- Russell, K.M., Galloway, J.N., Macko, S.A., Moody, J.L., Scudlark, J.R., 1998. Sources of nitrogen in wet deposition to the Chesapeake Bay region. Atmos. Environ. 32 (14–15), 2453–2465.
- Seinfeld, J.H., Pandis, S.N., 2012. Atmospheric Chemistry and Physics: from Air Pollution to Climate Change. Wiley, Hoboken, NJ.
- Seinfeld, J.H., Pandis, S.N., 2016. Atmospheric Chemistry and Physics: from Air Pollution to Climate Change. John Wiley & Sons.
- Seitzinger, S.P., Harrison, J.A., Dumont, E., Beusen, A., Bouwman, A.F., 2005. Sources and delivery of carbon, nitrogen, and phosphorus to the coastal zone: an overview of Global Nutrient Export from Watersheds (NEWS) models and their application. Global Biogeochem. Cycles 19 (4).
- Sigman, D.M., Fripiat, F., 2019. Nitrogen Isotopes in the Ocean, third ed. Academia, Encyclopedia of Ocean Sciences, pp. 263–278.
- Song, L., Walters, W.W., Pan, Y., Li, Z., Gu, M., Duan, Y., Lü, X., Fang, Y., 2021. 15N natural abundance of vehicular exhaust ammonia, quantified by active sampling techniques. Atmos. Environ. 255, 118430.
- Stein, A.F., Draxler, R.R., Rolph, G.D., Stunder, B.J.B., Cohen, M.D., Ngan, F., 2015. NOAA's HYSPLIT atmospheric transport and dispersion modeling system. Bull. Am. Meteorol. Soc. 96, 2059–2077.
- Walters, W.W., Chai, J., Hastings, M.G., 2019. Theoretical phase resolved Ammonia—Ammonium nitrogen equilibrium isotope exchange fractionations: applications for tracking atmospheric ammonia gas-to-particle conversion. ACS Earth Space Chem. 3, 79–89.
- Walters, W.W., Song, L., Chai, J., Fang, Y., Colombi, N., Hastings, M.G., 2020. Characterizing the spatiotemporal nitrogen stable isotopic composition of ammonia in vehicle plumes. Atmos. Chem. Phys. 20 (19), 11551–11567.
- Wang, Y.Q., Zhang, X.Y., Draxler, R., 2009. TrajStat: GIS-based software that uses various trajectory statistics analysis methods to identify potential sources from long-term air pollution measurement data. Environ. Model. Software 24, 938–939.
- Xiang, Y.-K., Dao, X., Gao, M., Lin, Y.-C., Cao, F., Yang, X.-Y., Zhang, Y.-L., 2022.
  Nitrogen isotope characteristics and source apportionment of atmospheric ammonium in urban cities during a haze event in Northern China Plain. Atmos. Environ. 269, 118800.
- Xiao, H.-W., Xiao, H.-Y., Shen, C.-Y., Zhang, Z.-Y., Long, A.-M., 2018. Chemical composition and sources of marine aerosol over the Western North Pacific Ocean in winter. Atmosphere 9 (298).
- Xiao, H.W., Xiao, H.Y., Long, A.M., Wang, Y.L., Liu, C.Q., 2013. Chemical composition and source apportionment of rainwater at Guiyang, SW China. J. Atmos. Chem. 70, 269–281.
- Xiao, H.W., Xiao, H.Y., Luo, L., Shen, C.Y., Long, A.M., Chen, L., Long, Z.H., Li, D.N., 2017. Atmospheric aerosol compositions over the South China Sea: temporal variability and source apportionment. Atmos. Chem. Phys. 17, 3199–3214.

- Xu, W., Zhao, Y., Wen, Z., Chang, Y., Pan, Y., Sun, Y., Ma, X., Sha, Z., Li, Z., Kang, J., Liu, L., Tang, A., Wang, K., Zhang, Y., Guo, Y., Zhang, L., Sheng, L., Zhang, X., Gu, B., Song, Y., Damme, M.V., Clarisse, L., Coheur, P.-F., Collett, J.L., Goulding, K., Zhang, F., He, K., Liu, X., 2022. Increasing importance of ammonia emission abatement in PM2.5 pollution control. Sci. Bull. 67, 1745–1749.
- Zhang, H.-H., Yang, G.-P., Liu, C.-Y., Su, L.-P., 2013. Chemical characteristics of aerosol composition over the Yellow Sea and the East China sea in autumn. J. Atmos. Sci. 70, 1784-1704
- Zhang, L., Altabet, M., Wu, T., Hadas, O., 2007. Sensitive measurement of NH4+ 15N/14N (d15NH4+) at natural abundance levels in fresh and saltwaters. Anal. Chem. 79, 5297–5303.
- Zhao, Y., Zhang, L., Pan, Y., Wang, Y., Paulot, F., Henze, D.K., 2015. Atmospheric nitrogen deposition to the northwestern Pacific: seasonal variation and source attribution. Atmos. Chem. Phys. 15 (9), 13657–13703.